ARTICLES

Dispersed Fluorescence Spectroscopy of S_0 Formyl Fluoride Vibrational States†

Katie M. Horsman, Todd P. Chassee, and William F. Polik*

Department of Chemistry, Hope College, Holland, Michigan 49423

Received: October 26, 1999; In Final Form: February 2, 2000

Dispersed fluorescence (DF) spectroscopy was used to record a 22 500 cm^{-1} spectrum of the vibrational energy levels of formyl fluoride (HFCO) and thereby determine harmonic frequencies and anharmonic constants for the S_0 potential energy surface. Sample molecules were cooled in a supersonic expansion and excited to low J, $K_a = 0$ rotational states in the 6^2 vibrational level of S_1 HFCO, and the resulting fluorescence was dispersed from 255 to 600 nm. Long progressions in the CO stretch ($\upsilon_2 = 0-6$) and out-of-plane bend ($\upsilon_6 = 0-23$) and shorter progressions in the CF stretch ($\upsilon_4 = 0-2$) and FCO bend ($\upsilon_5 = 0-2$) are observed. Analysis of the spectrum results in 240 assignments, including 196 new assignments and 56 assignments above the approximate 17 000 cm^{-1} dissociation threshold. The data are fit to an anharmonic oscillator model with a standard deviation of 3.3 cm^{-1}.

I. Introduction

Formyl fluoride (HFCO) is a particularly interesting molecule because of its relatively low dissociation barrier[1] of 17 000 cm^{-1}, which permits spectroscopic access to vibrational levels above the dissociation threshold. In contrast, formaldehyde (H_2CO) has a higher dissociation barrier[2] of 27 700 cm^{-1}, resulting in fluorescence to levels only well below the reaction threshold.[3] This work reports a comprehensive analysis of the S_0 vibrational level structure of HFCO, which can be utilized to model the potential energy surface below and above the barrier to dissociation.

The low-energy vibrational spectrum of HFCO was studied between 500 and 5000 cm^{-1} by Stratton and Nielsen[4] with medium resolution infrared spectroscopy, resulting in the assignment of five of the fundamental transition frequencies. Subsequent studies were carried out by Wong et al.[5] and by Kattenberg et al.[6] at higher resolution. More recently, the high-energy vibrational spectrum of HFCO was studied between 13 000 and 22 550 cm^{-1} by Choi and Moore[7] who used stimulated emission pumping (SEP) to assign 48 transitions. This work formed the basis for determining the dependence of the HFCO unimolecular dissociation rate on out-of-plane vibration and molecular rotation[8] and for measuring CO product state distributions[9,10] by Moore and co-workers. Theoretical studies of HFCO at the MP2 6-31Gext level have been carried out by Green et al.,[11] in which harmonic vibrational frequencies and anharmonic constants were calculated.

The current study uses dispersed fluorescence (DF) spectroscopy to characterize the S_0 vibrational structure of HFCO, as shown in Figure 1. In contrast to stimulated emission pumping (SEP), DF spectroscopy is a zero background technique and is not subject to saturation effects. Thus, dispersed fluorescence spectroscopy typically results in a higher signal-to-noise ratio and a wider dynamic range. While DF spectra are lower in resolution than SEP spectra, they can be recorded much more rapidly and cover a much wider spectral range.[12]

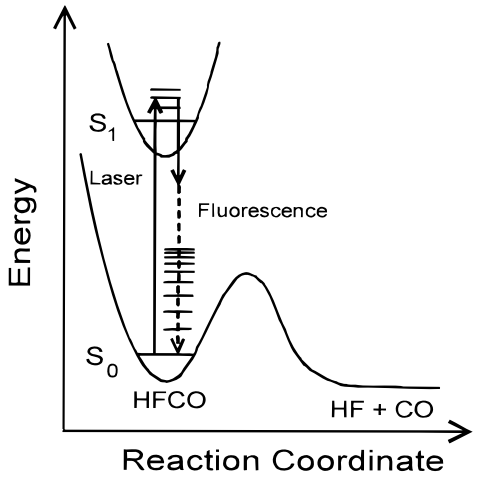

Figure 1. Dispersed fluorescence (DF) technique for HFCO. A laser excites a narrow range of rotational states in 6^2 S_1 HFCO. The resulting fluorescence to vibrational levels below and above the dissociation threshold is dispersed with a monochromator.

In the present work, a 22 500 cm^{-1} DF spectrum of S_0 HFCO was recorded, which includes the previously studied low- and high-energy regions and the unstudied intermediate energy region. The spectrum is assigned using harmonic oscillator basis states with anharmonic corrections. This analysis results in a 5-fold increase in the number of assignments compared to previous literature as well as correction of several misassignments. In addition to significantly increasing the total number of vibrational assignments, 56 assignments have been made above the dissociation threshold of HFCO to HF + CO near 17 000 cm^{-1}. It is significant to the dissociation dynamics that the vibrational levels above the dissociation barrier observed

† Part of the special issue "C. Bradley Moore Festschrift".

* To whom correspondence should be addressed. E-mail: polik@hope.edu.

10.1021/jp993794g CCC: $19.00
Published on Web 04/29/2000

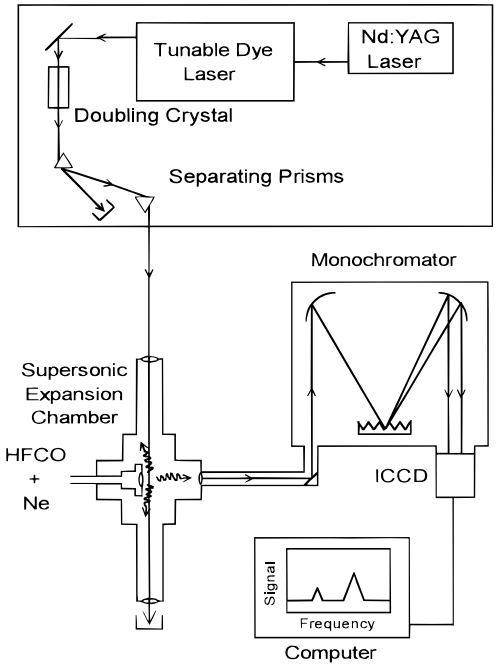

Figure 2. Schematic of experimental apparatus for recording the dispersed fluorescence (DF) spectrum of HFCO.

in this study are still well fit using an anharmonic oscillator model without extensive mixing of the harmonic oscillator basis states. Thus, the excited vibrational state structure of HFCO will serve as an important test for methods of calculating potential energy surfaces and for theories of unimolecular dissociation.

II. Experimental Section

Formyl fluoride was prepared from formic acid and cyanuric fluoride in acetonitrile using pyridine as a catalyst according to the method of Olah et al.[13] The HFCO was isolated by flowing the gas product through a −10 °C trap (H_2O/NaCl), which collected acetonitrile solvent and other condensable side products. A −130 °C trap (*n*-pentane slush) condensed the HFCO as a liquid while allowing the CO side product to pass by as a gas. The HFCO was freeze−pump−thawed and then purified by vacuum distillation at −78 °C (CO_2/ethanol) from the trap to a storage finger at −196 °C (liquid nitrogen) and kept for later use.

The experimental setup is schematically represented in Figure 2. A Nd:YAG laser (Lumonics HY 1200) produced 355 nm UV light and pumped a dye laser (Lumonics HD-300) using Coumarin 500 dye. The pulsed output near 510 nm was 10 ns in duration, about 14 mJ in energy, and 0.08 cm^{-1} in line width. This was frequency doubled with a 51° BBO doubling crystal (Quantum Technology) to produce 255 nm light. The ultraviolet light was separated from the residual, undoubled visible light with a pair of 60° quartz prisms and directed with two 90° quartz prisms through a 1 m focal length collimating lens and baffle arms into the molecular beam chamber, where the energy was measured to be 1.9 mJ with a pyroelectric detector (Molectron J4-09) connected to an energy meter (Molectron J1000).

The formyl fluoride was vacuum distilled to a Pyrex U-tube and maintained at −68 °C (chloroform slush), corresponding to a vapor pressure of 66 Torr. Neon carrier gas flowed over the HFCO with a 1.5 atm backing pressure and into a pulsed nozzle (General Valve series 9) with a 0.76 mm diameter orifice, which was raised 1 cm above the laser beam path and directed

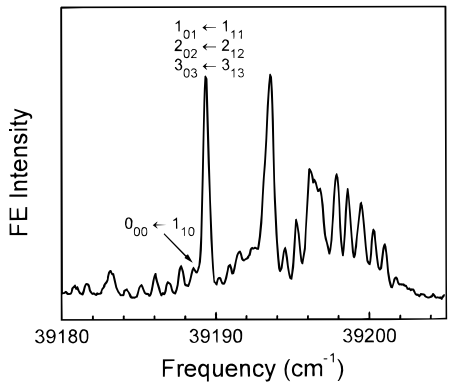

Figure 3. Fluorescence excitation (FE) spectrum of 6^2 S_1 HFCO. The 0_{00} rotational level is relatively weak and not well-resolved. The intense ${}^pQ_1(J'')_o$ branch is used to prepare the 1_{01}, 2_{02}, and 3_{03} states in 6^2 S_1 HFCO.

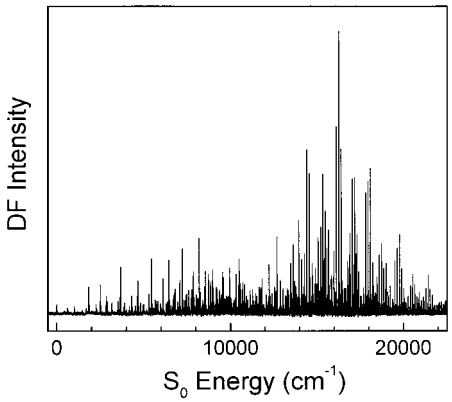

Figure 4. Dispersed fluorescence (DF) spectrum recorded from the ${}^pQ_1(J'')_o$ branch of the 6^2 vibrational state of S_1 HFCO. The abscissa scale is adjusted to read in S_0 rovibrational energy.

downward into a 6-in. diffusion pump (Edwards Diffstak 160). The HFCO was cooled by supersonic expansion to approximately 5 K, as determined by rotational structure in the fluorescence excitation spectrum.

The laser was tuned to the ${}^pQ_1(J'')_o$ branch at 39 189.3 cm^{-1} to excite the overlapping $1_{01} \leftarrow 1_{11}$, $2_{02} \leftarrow 2_{12}$, $3_{03} \leftarrow 3_{13}$ rotational transitions in the 6_0^2 $S_1 \leftarrow S_0$ vibronic band. These transitions are not saturated at the energy available from the laser system. The total fluorescence excitation (FE) intensity was monitored with a UV sensitive photomultiplier tube (Thorn EMI 9954B) positioned perpendicular to the laser and molecular beam axes. A Schott KV-370 filter was used to discriminate against scattered laser light, and Schott NG filters ($T = 0.002$) were used to reduce signal intensity before the photomultiplier tube. The FE signal from the PMT was averaged with a gated integrator (Standard Research Systems SR250), digitized (Keithly/Metrabyte DAS8-PGA), and stored on a personal computer.

Fluorescence was collected with a 12-in. focal length 1.5-in. diameter quartz lens, directed with a pair of mirrors through light baffles, and imaged with an 8-in. focal length 1.5-in. diameter quartz lens onto a 1 cm high × 600 μm wide entrance slit of a 1.25 m monochromator (SPEX 1250) with a 120 mm × 140 mm 2400 groove/mm holographic diffraction grating. The slit width of 600 μm was selected to maximize the signal while keeping vibronic lines resolved. A Schott KV-418 order-sorting filter was in place for measurements above 5000 Å. The fluorescence was monitored with an intensified charge coupling device (ICCD) detector (Princeton Instruments ICCD-576LDG/

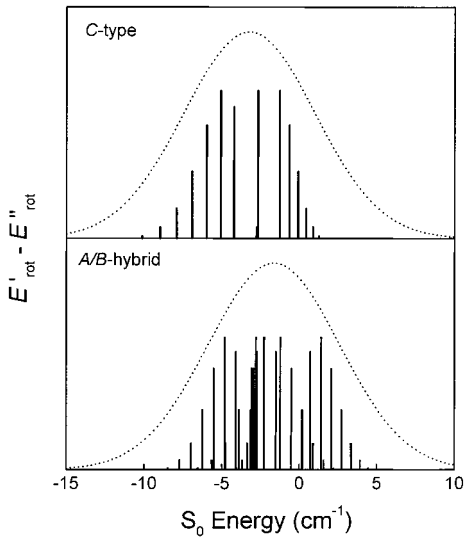

Figure 5. Calculated rotational transition frequencies and fluorescence intensities for excitation of the $6^2\ {}^pQ_1(J'')_o$ branch at 5 K (solid lines) compared to the 10 cm^{-1} instrumental resolution (dotted line). The rotational structure is entirely contained within the instrumental resolution, ensuring that every peak in the DF spectrum corresponds to a different S_0 level.

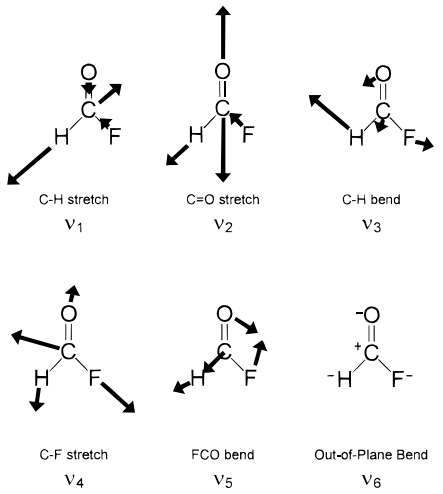

Figure 6. Six normal vibrational modes of formyl fluoride (HFCO).

RB) placed at the exit plane of the monochromator. The DF signal was recorded on 576 channels that spanned approximately 55 Å in first order. The ICCD gate width was 500 ns, and the dispersed fluorescence signal was summed for 2000 laser pulses. The dispersed fluorescence spectrum was recorded from 2500 to 6000 Å in the first order. The fwhm line width was observed to be 1.87 Å, which is consistent with the specified monochromator resolution of 1.95 Å with a 600 μm slit width and 2400 g/mm grating.

The DF spectrum was calibrated using an iron hollow cathode lamp (Fisher-Scientific) for wavelengths less than 2800 Å and a neon−thorium hollow cathode lamp for wavelengths greater than 2800 Å. Immediately after each 55 Å interval and prior to moving the diffraction grating, the monochromator slit width was reduced to 100 μm and a calibration spectrum was recorded. Iron, thorium, and neon transitions in the calibration spectra were assigned using MIT Fe wavelength tables[14] and LANL Atlas of the Thorium Spectrum.[15] The dispersion (wavelength vs ICCD pixel position) was fit to a fourth-order polynomial in order to account for its slight nonlinear behavior. Small systematic deviations from the dispersion curve were observed

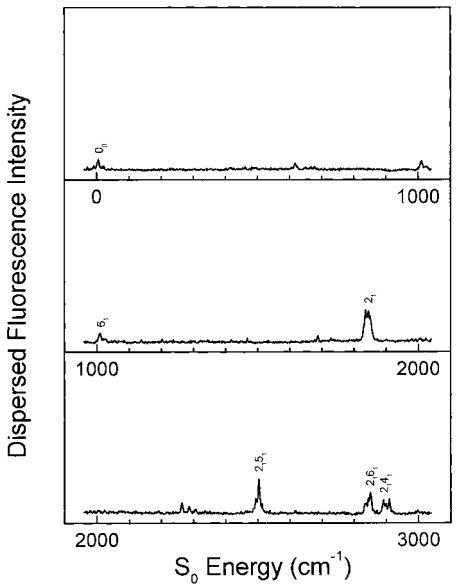

Figure 7. Dispersed fluorescence (DF) spectrum and vibrational assignments of S_0 HFCO. The spectrum was recorded from the $^pQ_1(J'')_o$ branch of the 6^2 vibrational state of S_1 HFCO. The abscissa scale is adjusted to read in S_0 rovibrational energy.

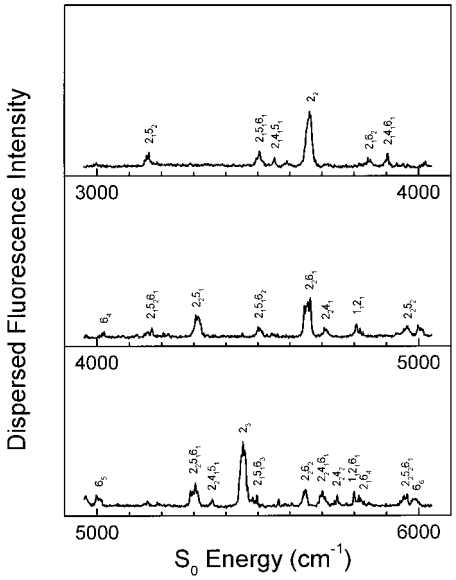

Figure 8. Dispersed fluorescence spectrum and vibrational assignments of S_0 HFCO. See Figure 7 caption.

as a function of pixel position, suggesting a slight nonuniformity in pixel spacing or the minifier of the ICCD. These systematic differences were fit to a third-order polynomial and a correction was applied. The standard deviation between the fitted calibration lines and their literature positions was 0.024 Å (0.097 cm^{-1} at 5000 Å), which is a measure of the accuracy of the apparatus and calibration procedure.

III. Results

A. Excitation of $K_a = 0$ 6^2 S_1 Formyl Fluoride. A fluorescence excitation (FE) spectrum was recorded from the ground vibrational state of S_0 HFCO to the 6^2 vibrational state of S_1 HFCO. The FE spectrum, shown in Figure 3, was assigned using the spectral prediction program ASYROT[16] with the spectroscopic parameters determined by Wong et al.[5] and Fischer et al.[17] To record the least conjested dispersed fluores-

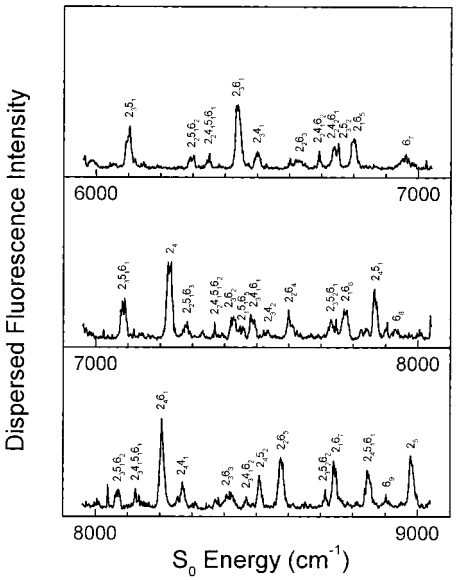

Figure 9. Dispersed fluorescence spectrum and vibrational assignments of S_0 HFCO. See Figure 7 caption.

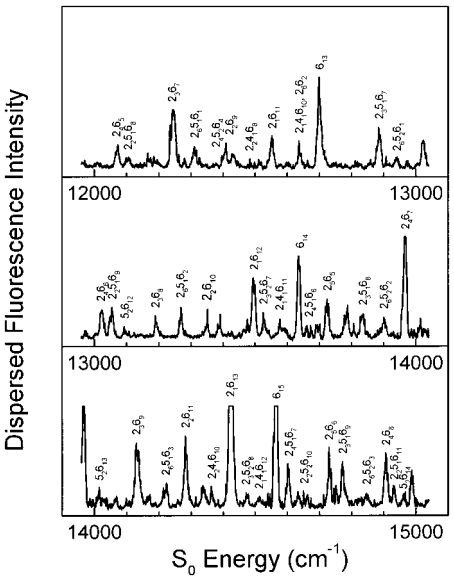

Figure 11. Dispersed fluorescence spectrum and vibrational assignments of S_0 HFCO. See Figure 7 caption.

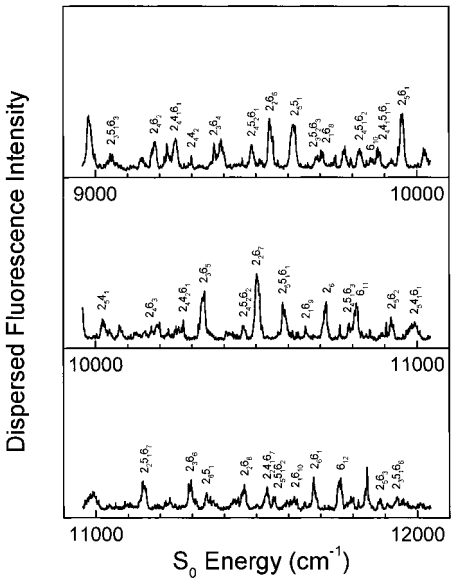

Figure 10. Dispersed fluorescence spectrum and vibrational assignments of S_0 HFCO. See Figure 7 caption.

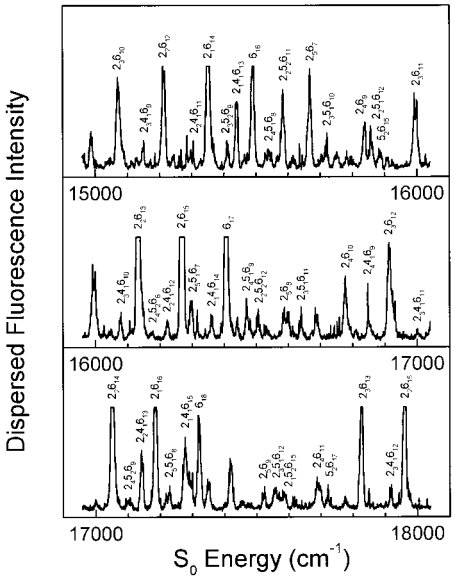

Figure 12. Dispersed fluorescence spectrum and vibrational assignments of S_0 HFCO. See Figure 7 caption.

cence (DF) spectrum, it is desirable to excite a single rovibrational level in S_1, preferably 0_{00}, so that rotational selection rules minimize the number of possible fluorescing transitions.[12] In the case of 6^2 S_1 HFCO, however, the 0_{00} transition is relatively weak in the present supersonic expansion conditions and is partially overlapped by the strong neighboring $^pQ_1(J'')_o$ branch, as can be seen in Figure 3. Consequently, the $^pQ_1(J'')_o$ branch was excited which prepares the 1_{01}, 2_{02}, and 3_{03} states in S_1. Although several states are initially prepared, the DF spectrum remains relatively unconjested for reasons discussed below.

B. Dispersed Fluorescence Spectroscopy of S_0 Formyl Fluoride. A dispersed fluorescence (DF) spectrum was recorded from the $^pQ_1(J'')_o$ branch of the 6^2 vibrational state in S_1 HFCO and is presented in Figure 4. The signal-to-noise ratio is observed to be approximately 250:1. The 22 500 cm^{-1} range of the DF spectrum extends well past the estimated 17 000 cm^{-1} barrier for HFCO dissociation to HF and CO.

Electric-dipole selection rules allow only a limited number of transitions from the 1_{01}, 2_{02}, and 3_{03} rotational levels of S_1 HFCO to each vibrational level of S_0 HFCO. In the C_s point group, the S_0 and S_1 electronic states have A′ and A″ electronic symmetry, respectively. In each of the S_0 and S_1 electronic states, the vibrational states for which v_6 is even have A′ symmetry, and vibrational states for which v_6 is odd have A″ symmetry. Electric dipole transitions are divided into *A*-type, *B*-type, and *C*-type transitions. In the $S_0 \leftrightarrow S_1$ electronic transition of HFCO, *A*/*B*-hybrid transitions occur between vibrational states where Δv_6 is odd and *C*-type transitions occur between vibrational states where Δv_6 is even. For a near-prolate top like HFCO, the rotational selection rules are $\Delta J = 0, \pm 1$, $\Delta K_a = 0$, and $\Delta K_c = \pm 1$ for an *A*-type transition; $\Delta J = 0, \pm 1$, $\Delta K_a = \pm 1$, and $\Delta K_c = \pm 1$ for a *B*-type transition; and $\Delta J = 0, \pm 1$, $\Delta K_a = \pm 1$, and $\Delta K_c = 0$ for a *C*-type transition.[18]

For *C*-type transitions, there are two possible transitions from each of the three populated rotational levels of 6^2 S_1 HFCO. The 1_{01} rotational levels can fluoresce only to the 2_{12} and 1_{11} rotational levels of S_0 HFCO. Similarly, the 2_{02} and 3_{03} rotational levels of 6^2 S_1 HFCO can fluoresce only to 3_{12} and 2_{11} and to

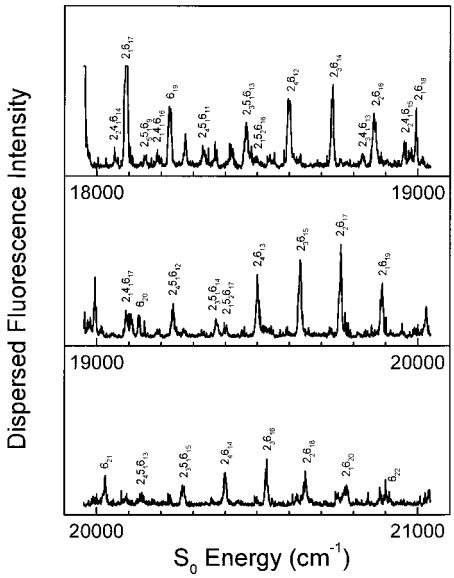

Figure 13. Dispersed fluorescence spectrum and vibrational assignments of S_0 HFCO. See Figure 7 caption.

4_{14} and 3_{13}, respectively. Although the energies of the 1_{01}, 2_{02}, and 3_{03} excited levels differ significantly, fluorescence wavelengths from these levels do not vary as much because higher energy excited states fluoresce to higher energy lower states, as discussed quantitatively below. For *A*/*B*-hybrid transitions, more fluorescence transitions are possible; however, their wavelengths do not vary much for similar reasons. At the resolution of the monochromator used in this work, the result is that *each vibrational state in S_0 is associated with a single peak in the dispersed fluorescence spectrum*. Such DF spectra may be termed *pure vibrational spectra* because they are free from rotational congestion at the recorded resolution. The energy of each observed S_0 vibrational level was determined by subtracting the energy of the fluorescence and the estimated rotational energy from the vibronic and rotational energy of the S_1 excited state

$$E''_{\text{vib}} = E'_{\text{vibronic}} + E'_{\text{rot}} - E_{\text{fluorescence}} - E''_{\text{rot}} \qquad (1)$$

where the single and double primes represent the upper and lower states, respectively.

Application of eq 1 is complicated by the fact that the laser excites a band of overlapped transitions. Despite the preparation of several S_1 rotational levels, the DF spectrum exhibits surprisingly narrow lines with very little rotational congestion. The quantity $E'_{\text{rot}} - E''_{\text{rot}}$ was modeled with the ASYROT spectral prediction program[16] using S_0 rotational constants from Wong et al.[5] and S_1 rotational constants from Fischer.[17] Since the excitation transition populates several $K_a = 0$ levels in S_1, the calculated transition frequencies were weighted by their absorption intensity at 5 K and by their fluorescence intensity. A weighted average and standard deviation of $E'_{\text{rot}} - E''_{\text{rot}}$ was calculated. Choi and Moore[7] found that the *A* rotational constant has a strong dependence on v_6 due to the strong Coriolis coupling between ν_4 and ν_6. Thus, the calculation was repeated at several values of ν_6 using the experimental value of $\alpha_6^A = 0.054$ cm^{-1} reported in ref 11 to describe the dependence of the effective *A* rotational constant on v_6 and consequently the v_6 dependence of $E'_{\text{rot}} - E''_{\text{rot}}$. For *C*-type transitions, the weighted average for even v_6'' is

$$E'_{\text{rot}} - E''_{\text{rot}} = -3.24\ \text{cm}^{-1} + 0.049 v_6''\ \text{cm}^{-1} \qquad (2a)$$

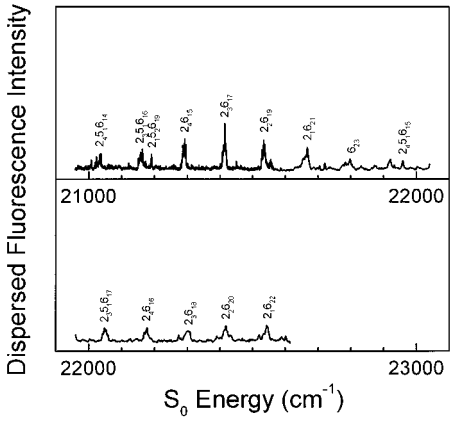

Figure 14. Dispersed fluorescence spectrum and vibrational assignments of S_0 HFCO. See Figure 7 caption.

with a weighted standard deviation of 1.8 cm^{-1}. For *A*/*B*-hybrid transitions, the weighted average value for odd v_6'' is

$$E'_{\text{rot}} - E''_{\text{rot}} = -1.46\ \text{cm}^{-1} + 0.023 v_6''\ \text{cm}^{-1} \qquad (2b)$$

with a weighted standard deviation of 2.6 cm^{-1}.

These small standard deviations are manifested in the spectrum by a relatively narrow band of overlapping rotational transitions within each vibronic transition. The contribution of overlapping rotational transitions to the observed line width is less than the instrumental resolution, which is determined by the entrance slit width to be 10 cm^{-1} at 16 000 cm^{-1} of S_0 energy, corresponding to the largest peak in the spectrum. The rotational transition frequencies and intensities are compared to the instrumental resolution in Figure 5. The combination of narrow rotational structure bandwidth and monochromator detection bandwidth ensures that every peak in the DF spectrum corresponds to a different S_0 level.

C. Vibrational Assignments. The six vibrational normal modes of HFCO as computed by MOPAC[19] are shown in Figure 6. Vibrational assignments are indicated on the DF spectrum from 6^2 S_1 HFCO in Figures 7−14. These transitions were assigned by considering their frequencies, relative spacing, and relative intensities within a series. The strongest transitions were first assigned to 2_m6_n. The remaining weaker transitions were assigned to $2_m6_n4_1$, $2_m6_n4_2$, $2_m6_n5_1$, $2_m6_n5_2$, and $2_m6_n4_15_1$. Excitation of a nonbonding electron on oxygen to a π^* antibonding orbital in HFCO increases the length of the C═O bond and causes the molecule to become pyramidal. According to the Franck−Condon principle, transitions in which substantial geometry changes occur will be most prominent in the spectrum, resulting in long progressions in ν_2 and ν_6. Smaller progressions were observed in ν_4 and ν_5 as a result of the involvement of the fluorine p orbital in the molecular π system. No transitions involving ν_3 and only two transitions involving ν_1 were observed due to the lack of σ bond involvement in the π system.

Table 1 shows the compilation of the vibrational assignments, observed frequencies, and calculated frequencies. States involving ν_1 were not included in the fit because there were not enough observations to confidently determine the harmonic frequency ω_1^0 and anharmonic corrections involving ν_1. A high-energy perturbation was identified involving $2_35_16_{n=10,11}$ and $2_45_16_{n=11-13}$, which is likely due to local tuning of a resonance interaction by the anharmonic constants. These states were excluded from the fit so as not to skew the resulting spectroscopic constants that assume the existence of only small perturbations.

TABLE 1: Vibrational State Assignments and Positions (cm^{-1}) for S_0 HFCO and Comparison to Anharmonic Fit Calculated Frequencies

assignment	frequency	calculated frequency	difference	assignment	frequency	calculated frequency	difference
0_0	0.2	0.0	−0.2	$2_4 4_2$	9294.1	9294.9	0.8
6_1	1007.0	1011.5	4.5	$2_3 6_4$	9364.8	9367.4	2.6
2_1	1836.1	1838.2	2.1	$2_4 5_2 6_1$	9484.1	9484.6	0.5
$2_1 5_1$	2498.9	2497.6	−1.3	$2_2 6_6$	9537.6	9540.5	2.9
$2_1 6_1$	2844.1	2841.7	−2.4	$2_5 5_1$	9610.9	9608.7	−2.2
$2_1 4_1$	2895.2	2896.3	1.1	$2_3 5_2 6_3$	9686.5	9688.3	1.8
1_1	2976.4[a]	2981.0[b]	4.6[c]	$2_1 6_8$	9700.6	9702.3	1.7
$2_1 5_2$	3153.2	3158.7	5.5	$2_4 5_1 6_2$	9818.2	9818.7	0.5
$2_1 5_1 6_1$	3501.7	3500.7	−1.0	6_{10}	9855.2	9855.6	0.4
$2_1 4_1 5_1$	3547.0	3547.1	0.1	$2_4 4_1 5_1 6_1$	9877.3	9876.5	−0.8
2_2	3656.5	3654.4	−2.1	$2_5 6_1$	9948.6	9950.7	2.1
$2_1 6_2$	3843.0	3839.5	−3.5	$2_5 4_1$	10019.1	10016.2	−2.9
$2_1 4_1 6_1$	3899.9	3896.4	−3.6	$2_4 6_3$	10149.1	10149.3	0.2
6_4	4017.0	4011.5	−5.5	$2_4 4_2 6_1$	10269.9	10269.6	−0.3
$2_1 5_2 6_1$	4166.7	4161.3	−5.4	$2_3 6_5$	10334.5	10331.6	−2.9
$2_2 5_1$	4307.3	4307.2	−0.1	$2_4 5_2 6_2$	10456.4	10459.2	2.8
$2_1 5_1 6_2$	4499.8	4497.9	−1.9	$2_2 6_7$	10499.8	10500.4	0.6
$2_2 6_1$	4651.9	4650.4	−1.5	$2_5 5_1 6_1$	10583.5	10583.4	−0.2
$2_2 4_1$	4706.3	4708.2	1.9	$2_1 6_9$	10650.8	10658.7	7.9
$1_1 2_1$	4801.8	4817.9[b]	16.1[c]	2_6	10710.8	10708.1	−2.7
$2_2 5_2$	4959.2	4961.8	2.6	$2_4 5_1 6_3$	10785.6	10787.5	1.9
6_5	5000.4	5000.0	−0.4	6_{11}	10808.3	10809.2	0.9
$2_2 5_1 6_1$	5298.7	5302.8	4.1	$2_5 6_2$	10914.7	10919.5	4.8
$2_2 4_1 5_1$	5353.1	5352.4	−0.7	$2_5 4_1 6_1$	10985.8	10987.8	2.0
2_3	5449.7	5449.0	−0.7	$2_2 5_1 6_7$	11146.3	11149.7	3.4
$2_1 5_1 6_3$	5494.2	5489.3	−4.9	$2_3 6_6$	11291.6	11289.7	−2.0
$2_2 6_2$	5643.0	5640.4	−2.6	$2_6 5_1$	11339.2	11334.8	−4.4
$2_2 4_1 6_1$	5698.0	5700.6	2.6	$2_2 6_8$	11457.8	11454.2	−3.6
$2_2 4_2$	5742.1	5744.2	2.1	$2_2 4_1 6_7$	11530.2	11529.2	−1.0
$1_1 2_1 6_1$	5796.8	5805.9[b]	9.1[c]	$2_5 5_1 6_2$	11550.1	11551.7	1.6
$2_1 6_4$	5815.5	5817.4	1.9	$2_1 6_{10}$	11613.3	11609.0	−4.3
$2_2 5_2 6_1$	5955.3	5956.8	1.5	$2_6 6_1$	11676.2	11677.0	0.8
6_6	5983.4	5982.8	−0.6	6_{12}	11755.0	11756.8	1.8
$2_3 5_1$	6095.4	6095.3	−0.1	$2_5 6_3$	11882.5	11881.9	−0.6
$2_2 5_1 6_2$	6292.1	6292.3	0.2	$2_3 5_1 6_6$	11932.6	11932.9	0.3
$2_2 4_1 5_1 6_1$	6346.4	6344.3	−2.1	$2_4 6_5$	12068.5	12069.1	0.6
$2_3 6_1$	6435.9	6437.8	1.9	$2_2 5_1 6_8$	12100.0	12103.0	3.0
$2_3 4_1$	6496.0	6498.5	2.5	$2_3 6_7$	12241.1	12241.5	0.4
$2_2 6_3$	6624.9	6624.5	−0.4	$2_6 5_1 6_1$	12307.8	12303.1	−4.7
$2_2 4_1 6_2$	6688.5	6687.1	−1.4	$2_2 6_9$	12406.3	12401.9	−4.4
$2_2 4_2 6_1$	6736.1	6733.1	−3.1	$2_2 4_1 6_8$	12479.9	12479.4	−0.5
$2_3 5_2$	6748.0	6743.3	−4.7	$2_1 6_{11}$	12550.3	12553.3	3.0
$2_1 6_5$	6797.5	6797.5	0.0	$2_6 6_2$	12632.5	12639.3	6.8
6_7	6958.0	6959.7	1.7	6_{13}	12696.7	12698.6	1.9
$2_3 5_1 6_1$	7082.9	7083.6	0.7	$2_3 5_1 6_7$	12883.3	12884.2	0.9
2_4	7224.9	7222.6	−2.3	$2_6 5_2 6_1$	12936.8	12930.9	−5.9
$2_2 5_1 6_3$	7277.9	7275.8	−2.1	$2_4 6_6$	13019.1	13019.5	0.4
$2_2 4_1 5_1 6_2$	7326.3	7330.3	4.0	$2_2 5_1 6_9$	13050.4	13050.2	−0.2
$2_3 6_2$	7423.9	7420.5	−3.4	$2_3 6_8$	13185.1	13187.1	2.0
$2_1 5_1 6_5$	7454.9	7454.4	−0.5	$2_6 5_1 6_2$	13264.4	13264.9	0.5
$2_3 4_1 6_1$	7483.6	7483.7	0.1	$2_2 6_{10}$	13347.3	13343.5	−3.8
$2_3 4_2$	7529.6	7530.1	0.5	$2_1 6_{12}$	13491.9	13491.6	−0.3
$2_2 6_4$	7594.4	7602.6	8.2	$2_3 5_2 6_7$	13524.7	13528.6	3.9
$2_3 5_2 6_1$	7728.4	7731.1	2.7	$2_1 4_1 6_{11}$	13574.1	13572.2	−1.9
$2_1 6_6$	7770.4	7771.7	1.3	6_{14}	13631.5	13634.4	2.9
$2_4 5_1$	7862.3	7862.3	0.0	$2_4 5_1 6_6$	13656.1	13656.2	0.1
6_8	7934.3	7930.9	−3.4	$2_5 6_5$	13782.5	13787.4	4.9
$2_3 5_1 6_2$	8064.6	8065.8	1.2	$2_3 5_1 6_8$	13829.2	13829.3	0.1
$2_3 4_1 5_1 6_1$	8121.3	8120.8	−0.5	$2_6 5_2 6_2$	13897.3	13892.2	−5.1
$2_4 6_1$	8202.7	8204.4	1.7	$2_4 6_7$	13964.9	13963.6	−1.3
$2_4 4_1$	8266.3	8267.7	1.4	$5_2 6_{13}$	14011.6	14019.0	7.4
$2_3 6_3$	8404.6	8397.0	−7.6	$2_3 6_9$	14129.5	14126.4	−3.1
$2_3 4_1 6_2$	8464.2	8462.8	−1.5	$2_6 5_1 6_3$	14220.5	14220.2	−0.3
$2_4 5_2$	8505.4	8503.8	−1.6	$2_2 6_{11}$	14280.1	14278.9	−1.2
$2_2 6_5$	8573.1	8574.6	1.5	$2_2 4_1 6_{10}$	14359.4	14361.5	2.1
$2_3 5_2 6_2$	8709.9	8712.7	2.8	$2_1 6_{13}$	14422.8	14423.9	1.1
$2_1 6_7$	8738.4	8740.0	1.6	$2_3 5_2 6_8$	14470.5	14473.2	2.7
$2_4 5_1 6_1$	8845.0	8843.7	−1.3	$2_1 4_1 6_{12}$	14508.1	14506.9	−1.2
6_9	8900.2	8896.2	−4.0	6_{15}	14561.2	14564.3	3.1
2_5	8973.7	8975.5	1.8	$2_4 5_1 6_7$	14600.6	14599.7	−0.9
$2_3 5_1 6_3$	9042.7	9041.8	−0.9	$2_2 5_2 6_{10}$	14647.5	14640.7	−6.8
$2_4 6_2$	9180.1	9180.0	−0.1	$2_5 6_6$	14726.6	14730.5	3.9
$2_4 4_1 6_1$	9245.5	9245.9	0.4	$2_3 5_1 6_9$	14769.2	14768.1	−1.1

TABLE 1: Continued

assignment	frequency	calculated frequency	difference	assignment	frequency	calculated frequency	difference
$2_6 5_2 6_3$	14844.3	14847.0	2.7	$2_3 6_{13}$	17824.4	17821.0	−3.5
$2_4 6_8$	14902.0	14901.3	−0.8	$2_3 4_1 6_{12}$	17915.7	17913.3	−2.4
$2_2 5_1 6_{11}$	14929.1	14926.1	−3.0	$2_2 6_{15}$	17958.2	17958.7	0.5
$5_2 6_{14}$	14959.1	14953.8	−5.3	$2_2 4_1 6_{14}$	18051.2	18051.8	0.6
$2_3 6_{10}$	15065.2	15059.5	−5.7	$2_1 6_{17}$	18089.1	18092.0	2.9
$2_3 4_1 6_9$	15145.7	15143.7	−2.0	$2_5 5_1 6_9$	18147.9	18149.3	1.4
$2_2 6_{12}$	15209.7	15208.2	−1.6	$2_1 4_1 6_{16}$	18184.0	18185.1	1.1
$2_2 4_1 6_{11}$	15292.4	15293.4	1.0	6_{19}	18224.0	18223.8	−0.2
$2_1 6_{14}$	15347.4	15350.1	2.7	$2_4 5_1 6_{11}$	18326.7	18310.1	−16.6[c]
$2_3 5_2 6_9$	15408.2	15411.5	3.3	$2_3 5_1 6_{13}$	18463.2	18460.6	−2.6
$2_1 4_1 6_{13}$	15437.4	15435.6	−1.8	$2_1 5_2 6_{16}$	18492.8	18488.3	−4.5
6_{16}	15486.4	15488.2	1.8	$2_4 6_{12}$	18594.6	18588.0	−6.6
$2_4 5_1 6_8$	15533.7	15536.9	3.2	$2_3 6_{14}$	18731.5	18728.8	−2.7
$2_2 5_2 6_{11}$	15581.3	15575.1	−6.2	$2_3 4_1 6_{13}$	18825.9	18823.9	−2.0
$2_5 6_7$	15664.7	15667.1	2.4	$2_2 6_{16}$	18860.9	18863.0	2.1
$2_3 5_1 6_{10}$	15716.7	15700.7	−16.0[c]	$2_2 4_1 6_{15}$	18953.4	18958.8	5.4
$2_4 6_9$	15836.8	15832.6	−4.2	$2_1 6_{18}$	18990.8	18993.7	2.9
$2_2 5_1 6_{12}$	15852.6	15854.9	2.3	$2_1 4_1 6_{17}$	19087.1	19089.4	2.3
$5_2 6_{15}$	15882.7	15882.6	−0.1	6_{20}	19127.1	19123.6	−3.5
$2_3 6_{11}$	15992.6	15986.3	−6.3	$2_4 5_1 6_{12}$	19232.6	19221.6	−11.0[c]
$2_3 4_1 6_{10}$	16073.7	16073.2	−0.5	$2_3 5_1 6_{14}$	19368.6	19367.9	−0.7
$2_2 6_{13}$	16129.2	16131.2	2.0	$2_1 5_2 6_{17}$	19398.1	19395.1	−3.0
$2_4 5_2 6_8$	16170.4	16174.2	3.8	$2_4 6_{13}$	19497.6	19493.6	−4.0
$2_2 4_1 6_{12}$	16219.3	16219.1	−0.3	$2_3 6_{15}$	19632.3	19630.2	−2.1
$2_1 6_{15}$	16267.2	16270.2	3.0	$2_2 6_{17}$	19758.4	19761.2	2.8
$2_5 5_1 6_7$	16294.9	16296.7	1.8	$2_1 6_{19}$	19887.0	19889.2	2.2
$2_1 4_1 6_{14}$	16357.6	16358.2	0.6	6_{21}	20024.2	20017.3	−6.9
6_{17}	16404.7	16406.1	1.4	$2_4 5_1 6_{13}$	20138.1	20126.7	−11.4[c]
$2_4 5_1 6_9$	16467.0	16467.7	0.7	$2_3 5_1 6_{15}$	20265.6	20268.9	3.3
$2_2 5_2 6_{12}$	16502.4	16503.3	0.9	$2_4 6_{14}$	20394.3	20392.7	−1.6
$2_5 6_8$	16587.9	16597.2	9.3	$2_3 6_{16}$	20525.3	20525.3	0.0
$2_3 5_1 6_{11}$	16637.6	16627.0	−10.6[c]	$2_2 6_{18}$	20647.2	20653.0	5.8
$2_4 6_{10}$	16772.8	16757.5	−15.3[c]	$2_1 6_{20}$	20778.2	20778.6	0.4
$2_4 4_1 6_9$	16844.5	16845.4	0.9	6_{22}	20907.7	20904.9	−2.8
$2_3 6_{12}$	16909.0	16906.8	−2.2	$2_4 5_1 6_{14}$	21033.0	21025.2	−7.8
$2_3 4_1 6_{11}$	16997.5	16996.4	−1.1	$2_3 5_1 6_{16}$	21155.5	21163.4	7.9
$2_2 6_{14}$	17046.9	17048.1	1.2	$2_1 5_2 6_{19}$	21187.8	21190.3	2.5
$2_4 5_2 6_9$	17099.2	17104.5	5.3	$2_4 6_{15}$	21289.6	21285.3	−4.3
$2_2 4_1 6_{13}$	17139.9	17138.5	−1.4	$2_3 6_{17}$	21412.2	21414.0	1.8
$2_1 6_{16}$	17181.3	17184.1	2.8	$2_2 6_{19}$	21532.3	21538.5	6.2
$2_5 5_1 6_8$	17221.5	17226.3	4.8	$2_1 6_{21}$	21664.5	21661.7	−2.8
$2_1 4_1 6_{15}$	17275.3	17274.7	−0.6	6_{23}	21788.3	21786.5	−1.8
6_{18}	17318.1	17317.9	−0.2	$2_4 5_1 6_{15}$	21917.0	21917.3	0.3
$2_5 6_9$	17520.2	17520.8	0.6	$2_3 5_1 6_{17}$	22047.0	22051.6	4.6
$2_3 5_1 6_{12}$	17553.6	17547.0	−6.7	$2_4 6_{16}$	22171.5	22171.3	−0.2
$2_1 5_2 6_{15}$	17582.0	17575.4	−6.6	$2_3 6_{18}$	22296.7	22296.2	−0.5
$2_4 6_{11}$	17685.1	17676.0	−9.2	$2_2 6_{20}$	22413.9	22417.7	3.8
$5_2 6_{17}$	17719.7	17722.3	2.6	$2_1 6_{22}$	22540.1	22538.6	−1.5

[a] Not observed in spectrum; value from ref 11. [b] States involving ν_1 were calculated using $\omega_1^0 = 3041.6$ cm^{-1} and $x_{11} = -60.61$ cm^{-1} from ref 11. [c] Not included in fit.

The uncertainty in the S_0 vibrational energies depends on the accuracy of the fluorescence wavelength calibration and the precision with which the center of the spectral peaks can be determined. The fluorescence wavelength calibration was accurate to 0.1 cm^{-1}, and the center of the spectral peaks can be determined with an accuracy estimated at one-fifth of the line width or 2 cm^{-1}. Therefore, the uncertainty in the vibrational state energies is estimated to be 2 cm^{-1}, which is consistent with the observed 1.6 cm^{-1} standard deviation of the difference between S_0 vibrational energies determined by Choi and Moore using SEP and by this work.

A total of 240 assignments were made, including 56 assignments above the dissociation threshold of approximately 17 000 cm^{-1}. Of the 200 most intense lines observed in the spectrum, 179 were assigned. Thus, this work represents the most comprehensive set of S_0 vibrational assignments for HFCO to date.

IV. Discussion

A. Spectroscopic Vibrational Constants. The vibrational energy was calculated using the anharmonic oscillator model

$$E(\upsilon_1,\upsilon_2,...,\upsilon_n) = \sum_i \omega_i^0 \upsilon_i + \sum_{i\le j} x_{ij}\upsilon_i\upsilon_j + \sum_{i\le j\le k} y_{ijk}\upsilon_i\upsilon_j\upsilon_k \quad (3)$$

where ω_i^0 are normal mode harmonic vibrational frequencies, x_{ij} are first-order anharmonicity constants, y_{ijk} are second-order anharmonicity constants, n is the total number of normal modes, υ_i is the number of quanta in the ith normal mode, and the zero of energy is defined at the vibrationless level. The advantage of fitting to the ω_i^0 vibrational constants rather than to the harmonized ω_i constants is that each ω_i^0 constant is only affected by errors in the respective x_{ii} anharmonic constant, rather than in the x_{ij} anharmonic constants, which are not all determined.[20] Second-order anharmonicity corrections were used

TABLE 2: Spectroscopic Vibrational Constants for S_0 HFCO in cm^{-1}

	experiment		theory	states contributing
parameter	ref 7	this work	ref 11	to constant
ω_1^0		3041.6[a]	3160	0
ω_2^0	1848.79	1849.27(130)	1845	207
ω_3^0			1377	
ω_4^0		1071.46(271)	1043	44
ω_5^0		665.16(156)	651	84
ω_6^0	1013.86(56)	1014.29(35)	1027	206
x_{11}		−60.61[a]	−60.61	0
x_{12}			−1.20	
x_{13}			−21.19	
x_{14}			0.79	
x_{15}			0.64	
x_{16}			−15.62	
x_{22}	−12.00(39)	−11.19(54)	−10.81	164
x_{23}			−4.59	
x_{24}		−4.38(50)	−6.75	44
x_{25}		−6.56(23)	−4.79	80
x_{26}	−7.24(16)	−7.95(14)	−7.34	181
x_{33}			−8.90	
x_{34}			−8.79	
x_{35}			−1.34	
x_{36}			2.63	
x_{44}		−8.90(119)	−6.77	5
x_{45}		−8.66(176)	−8.10	6
x_{46}		−3.58(13)	−3.93	34
x_{55}		0.84(60)	−0.59	30
x_{56}		−0.51(6)	−1.10	72
x_{66}	−2.837(59)	−2.84(4)	−2.86	178
y_{222}	0.060(55)	0.071(57)		113
y_{226}	0.242(18)	0.152(21)		143
y_{266}	−0.117(7)	−0.068(6)		156
y_{666}	−0.0021(16)	−0.0033(13)		160

[a] Not determined by fit; values from ref 11.

for predicting the vibrational energy of states involving ν_2 and ν_6 because of the long progressions observed in these modes. Vibrational constants were not obtained for ν_1 and ν_3 because no progressions were observed involving these vibrations. The anharmonic oscillator fit parameters are shown in Table 2. The standard deviation of the fit was 3.3 cm^{-1}, which is slightly greater than the 2 cm^{-1} accuracy with which S_0 vibrational energies can be measured, suggesting only a very slight breakdown in the anharmonic oscillator model for these vibrational modes at these energies. In the work of Choi and Moore,[7] only progressions in ν_2 and ν_6 were assigned. In the present work, small progressions in ν_4 and ν_5 are also observed, permitting the calculation of previously undetermined constants.

The fit parameters are in good agreement with those determined by Choi and Moore. The parameter values obtained in this work overlap with those calculated by Choi and Moore within uncertainty limits, with the exception of x_{26}, y_{226}, and y_{266}. The significant difference in these values can be understood by the increased number of quantum states observed in this work as well as the misassignment of several 2_m6_n levels in the previous literature. There are minor discrepancies between the harmonic frequencies and anharmonic frequencies in comparison to theoretical calculations by Green et al.[11] The harmonic frequencies differ from the theoretical values by an average of 15 cm^{-1}, which corresponds to an average percent deviation of approximately 2%. The anharmonic constants differ by an average of 1 cm^{-1}.

Green et al. suggest that the influence of Fermi interactions and a Darling−Dennison resonance may have led to the discrepancies between the experimentally determined fit parameters of Choi and Moore and their theoretically determined fit parameters. The current data set, which covers a wider energy range and determines more constants, shows no evidence of pervasive Fermi or Darling−Dennison interactions, although local interactions were observed at high energy.

B. Comparison to Previous Assignments. Several discrepancies exist regarding the assignment of vibrational states in previous literature. Choi and Moore[7] report the position of 2_46_6 at 13 050.0 cm^{-1}. This work has found that the position of 2_46_6 is at 13 019 cm^{-1} and the vibrational state at 13 050 cm^{-1} is actually $2_25_16_9$. The line observed at 16 637.0 cm^{-1} and previously assigned to 2_56_8 is assigned here as $2_35_16_{11}$ and 2_56_8 is found at 16 588 cm^{-1}. The other two assignments by Choi and Moore involving 2_5 are 2_56_{13} and 2_56_{14}. In the present spectrum these two peaks are observed to be part of a longer progression, whose other members are not well fit by assignment to 2_56_n but are well fit by assignment to $2_35_16_{n+3}$. This leads to reassignment of the peak at 21 154.6 cm^{-1} from 2_56_{13} to $2_35_16_{16}$ and the peak at 22 046.1 cm^{-1} from 2_56_{14} to $2_35_16_{17}$. The improved set of assignments in the present work is due to the greater spectral coverage, which allows more complete progressions to be analyzed, and to the identification of weak progressions involving ν_4 and ν_5. Future work will focus on obtaining data from other vibrational states in order to access vibrational modes 1 and 3.

V. Conclusion

The dispersed fluorescence (DF) spectrum from 6^2 S_1 HFCO has increased the number of assigned vibrational states from 48 to 240, including 56 assignments over the approximate 17 000 cm^{-1} dissociation barrier. The set of assignments reported in this work permits the determination of previously unknown spectroscopic constants, as well as corrects several misassignments in previous literature. This larger set of assignments allows for the determination of additional vibrational spectroscopic constants, which will result in a better characterization of the molecular potential energy surface.

The 3.3 cm^{-1} standard deviation of the harmonic oscillator fit is only slightly larger than the 2 cm^{-1} accuracy of the S_0 vibrational energies. The vibrational structure of S_0 HFCO is well described by the anharmonic oscillator model, with no evidence of pervasive Fermi or Darling−Dennison interactions at the energies and for the vibrational modes studied.

Acknowledgment. The authors are indebted to Professor C. Bradley Moore for the training and guidance he provided and for his inspiring work on the spectroscopy and dynamics of small polyatomic molecules. K.M.H. acknowledges the Beckman Foundation for the receipt of a Beckman Scholar Award and T.P.C. acknowledges the Dreyfus Foundation for a summer research stipend. This research was supported by the Wyckoff Chemical Co. and National Science Foundation grant CHE9157713.

References and Notes

(1) Reid, S. A.; Reisler, H. *Annu. Rev. Phys. Chem.* **1996**, *47*, 495.
(2) Polik, W. F.; Guyer, D. R.; Moore, C. B. *J. Chem. Phys.* **1989**, *92*, 3453.
(3) Bouwens, R. J.; Hammerschmidt, J. A.; Grzeskowiak, M. M.; Stegink, T. A.; Yorba, P. M.; Polik, W. F. *J. Chem. Phys.* **1996**, *104*, 460.
(4) Stratton, R. F.; Nielsen, A. H. *J. Mol. Spectrosc.* **1960**, *4*, 373.
(5) Wong, M.; Johns, J. W. C.; McKellar, A. R. W. *J. Mol. Spectrosc.* **1982**, *94*, 79.
(6) Kattenberg, H. W.; Elst, R.; Oskam, A. *J. Mol. Spectrosc.* **1971**, *39*, 29.
(7) Choi, Y. S.; Moore, C. B. *J. Chem. Phys.* **1991**, *94*, 5414.

(8) Choi, Y. S.; Moore, C. B. *J. Chem. Phys.* **1992**, *97*, 1010.
(9) Choi, Y. S.; Teal, P.; Moore C. B. *J. Opt. Soc. Am. B* **1990**, *7*, 1829.
(10) Choi, Y. S.; Moore, C. B. *J. Chem. Phys.* **1995**, *103*, 9981.
(11) Green, W. H.; Jayatilaka, D.; Willetts, A.; Amos, R. D.; Handy, N. C. *J. Chem. Phys.* **1990**, *93*, 4965.
(12) Polik, W. F.; van Ommen, J. R. In *Highly Excited States: Relaxation, Reactions, and Structure*; Mullin, A. S., Schatz, G. C., Eds.; ACS Symposium Series 678; American Chemical Society: Washington, DC, 1997; p 51.
(13) Olah, G. A.; Kuhn, S. J. *J. Am. Chem. Soc.* **1960**, *82*, 2380.
(14) Phelps, F., III. *MIT Wavelength Tables Vol. 2: Wavelengths by Element*; The MIT Press: Cambridge, MA, 1991.
(15) Palmer, B., Engelman, R., Jr. *Atlas of the Thorium Spectrum*; Los Alamos National Laboratory: Los Alamos, 1983; LA-9615.
(16) Birss, F. W.; Ramsay, D. A. *Comput. Phys. Commun.* **1984**, *38*, 83.
(17) Fischer, G. *J. Mol. Spectrosc*. **1969**, *29*, 37.
(18) Herzberg, G. *Molecular Spectra and Molecular Structure III. Electronic Spectra and Electronic Structure of Polyatomic Molecules*; Van Nostrand Reinhold: New York, 1966; pp 244−8.
(19) Stewart, J. J. P. MOPAC 6.0, 1990.
(20) Herzberg, G. *Molecular Spectra and Molecular Structure II. Infrared and Raman Spectra of Polyatomic Molecules*; Van Nostrand Reinhold: New York, 1945; p 206, eq II, 270.